Title
Surface Dipole Control of Liquid Crystal Alignment

Journal
Journal of the American Chemical Society, 138(18)

ISSN
0002-7863

Authors
Schwartz, Jeffrey J
Mendoza, Alexandra M
Wattanatorn, Natcha
et al.

Publication Date
2016-05-11

DOI
10.1021/jacs.6b02026

Peer reviewed

JACS
JOURNAL OF THE AMERICAN CHEMICAL SOCIETY
Article
pubs.acs.org/JACS

Surface Dipole Control of Liquid Crystal Alignment

Jeffrey J. Schwartz,[†,‡] Alexandra M. Mendoza,[†,§] Natcha Wattanatorn,[†,§] Yuxi Zhao,[†,§] Vinh T. Nguyen,[§] Alexander M. Spokoyny,[*,§,⊥] Chad A. Mirkin,[*,⊥] Tomáš Baše,[*,∥] and Paul S. Weiss[*,†,§,#]

[†]California NanoSystems Institute, University of California, Los Angeles, Los Angeles, California 90095, United States
[‡]Department of Physics & Astronomy, University of California, Los Angeles, Los Angeles, California 90095, United States
[§]Department of Chemistry & Biochemistry, University of California, Los Angeles, Los Angeles, California 90095, United States
[⊥]Department of Chemistry and the International Institute for Nanotechnology, Northwestern University, Evanston, Illinois 60208, United States
[∥]Institute of Inorganic Chemistry, Academy of Sciences of the Czech Republic, v.v.i., č.p. 1001, 250 68 Husinec-Řež, Czech Republic
[#]Department of Materials Science & Engineering, University of California, Los Angeles, Los Angeles, California 90095, United States

Supporting Information

ABSTRACT: Detailed understanding and control of the intermolecular forces that govern molecular assembly are necessary to engineer structure and function at the nanoscale. Liquid crystal (LC) assembly is exceptionally sensitive to surface properties, capable of transducing nanoscale intermolecular interactions into a macroscopic optical readout. Self-assembled monolayers (SAMs) modify surface interactions and are known to influence LC alignment. Here, we exploit the different dipole magnitudes and orientations of carboranethiol and -dithiol positional isomers to deconvolve the influence of SAM-LC dipolar coupling from variations in molecular geometry, tilt, and order. Director orientations and anchoring energies are measured for LC cells employing various carboranethiol and -dithiol isomer alignment layers. The normal component of the molecular dipole in the SAM, toward or away from the underlying substrate, was found to determine the in-plane LC director orientation relative to the anisotropy axis of the surface. By using LC alignment as a probe of interaction strength, we elucidate the role of dipolar coupling of molecular monolayers to their environment in determining molecular orientations. We apply this understanding to advance the engineering of molecular interactions at the nanoscale.

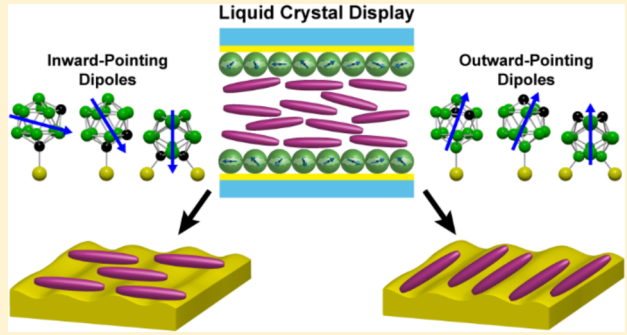

INTRODUCTION

Self-assembly plays critical roles in the development of materials with customized chemical and physical properties from the bottom up, and provides insights into molecular-scale phenomena.[1−4] Non-covalent interactions, including dipolar and dispersion forces, mediate molecular assembly and influence the properties and functions of pure and composite materials.[5−9] Understanding and controlling the types and strengths of these interactions, particularly at interfaces, enables engineering precisely tailored structures at the nanoscale.[10−15] Self-assembled monolayers (SAMs) not only exemplify these structures, but also serve as a powerful and versatile means of tuning the interactions of a surface with its surroundings and other molecular adsorbates.[16−19] A great deal of work has been done using SAMs to control the adsorption, position, orientation, and nucleation of crystalline and molecular assemblies.[20−26] Despite recent progress, however, predictive understanding of complex, extended assemblies across textured surfaces remains challenging.[27,28]

Liquid crystals (LCs) assemble with long-range orientational order due to anisotropic intermolecular interactions with their surroundings and are particularly sensitive to surface textures and coatings.[29−31] Industrially, LC alignment is controlled by unidirectional rubbing[32,33] or other techniques that break the rotational symmetry of the alignment surfaces.[34−36] One such alternative utilizes the dune-like surface texture of obliquely deposited, semi-transparent gold films[37,38] to direct LC alignment.[34,37,39−42] In this case, mesogens adopt in-plane orientations with their long axes perpendicular to the oblique deposition direction, minimizing elastic strain within the LC assembly.

Abbott and others have shown that SAMs also influence the alignment of LCs,[43−48] with the ability to control both azimuthal and polar orientations, which have found use in sensors.[49] However, a convolution of steric effects, surface topography, and intermolecular forces complicates our understanding of the mechanisms responsible for alignment.[46,47,50−52] Molecular adsorbates, in the form of either well-organized SAMs or adventitious surface contamination,

Received: February 23, 2016
Published: April 19, 2016

DOI: 10.1021/jacs.6b02026
J. Am. Chem. Soc. 2016, 138, 5957−5967

can alter LC arrangement by changing the preferred in-plane alignment axis or inducing homeotropic alignment, normal to the surface.[43,45,53] In the case of alignment layers treated with SAMs, different LC orientations have been observed using polar and nonpolar adsorbate molecules.[44,38,51] Additionally, chiral and "odd−even" [54] effects have been observed, showing that LC alignment is sensitive to variations in the symmetry[55−57] and orientation[46,47] of the exposed moieties of the terminal functionality of the SAM. Self-assembled adsorbates used in previous studies typically varied in two or more of these factors *simultaneously* (e.g., comparing structural analogues with different exposed moieties: $-CH_3$, −OH, and −COOH). As such, the independent effects of molecular geometry, orientation, and dipole moment on LC alignment are difficult to determine.

We used positional isomers of carboranethiol and -dithiol molecules[58] to deconvolve the effects of SAM dipole magnitude and orientation on the alignment of LCs. The isomers chemisorb onto gold surfaces through the formation of Au−S bonds, thereby assembling into monolayers with exposed carborane moieties. Each isomer possesses an identical molecular geometry and assembles "upright" with negligible tilt and a characteristic lattice spacing (7.2 and 7.6 Å for monothiol and dithiol species, respectively).[14,59−64] The primary attribute that distinguishes SAMs of each isomer is their different constituent dipole moments. Intermolecular forces between carboranethiol monolayers and mesogens resulted in uniaxial planar alignment of LCs along one of two distinct directions relative to the underlying anisotropic substrate: parallel or perpendicular to the oblique gold deposition direction ($\vec{\mathbf{Au}}$). The effects of these short-range, nanoscale forces[14,65] were transduced and amplified by the LCs to a macroscopic scale, enabling optical readout via transmitted light. Azimuthal anchoring energies of LCs on carboranethiol and -dithiol monolayers were measured to quantify SAM-LC coupling. This work targets and elucidates the roles of surface dipoles, in the form of adsorbed molecular dipoles, on the alignment and orientation of subsequent adsorbates (LCs), which has applications in sensing, catalysis, photovoltaics, and templated growth of nanostructures.[66−69] Self-assembled carboranethiols are well-suited to this purpose as they enable direct comparison of the effects of different isomers' molecular dipoles, while holding constant other factors influencing LC alignment that have confounded previous studies.

RESULTS AND DISCUSSION

Figure 1 illustrates the molecules used in these studies. Caboranethiol isomers *m*-9-carboranethiol (**M9**), *m*-1-carboranethiol (**M1**), *o*-9-carboranethiol (**O9**), *o*-1-carboranethiol (**O1**), and -dithiol isomers *o*-9,12-carboranedithiol (**9O12**) and *o*-1,2-carboranedithiol (**1O2**) possess dipole moments with various strengths and orientations.[70] The dipole moments of these six carboranethiols were calculated using density functional theory.[14,60,71,72] Although the molecular dipoles will be altered upon chemisorption to a gold surface,[73] we use these values to make qualitative comparisons of their relative strengths, their orientations, and the degree to which they modify the surface energy of a substrate through their dipolar fields.[60,72] We use two LCs, 4-cyano-4′-pentylbiphenyl (**5CB**) and *N*-(4-methoxybenzylidene)-4-butylaniline (**MBBA**), possessing oppositely signed dielectric anisotropies ($\Delta\varepsilon$), to probe these fields. Mesogens with positive $\Delta\varepsilon$ (**5CB**) align parallel to an applied electric field, whereas the long axes of mesogens with negative $\Delta\varepsilon$ (**MBBA**) align perpendicular to an applied field. Comparison of the alignment of **5CB** and **MBBA** on carboranethiol monolayers enables us to infer the role of the dipolar field on LC alignment.[43]

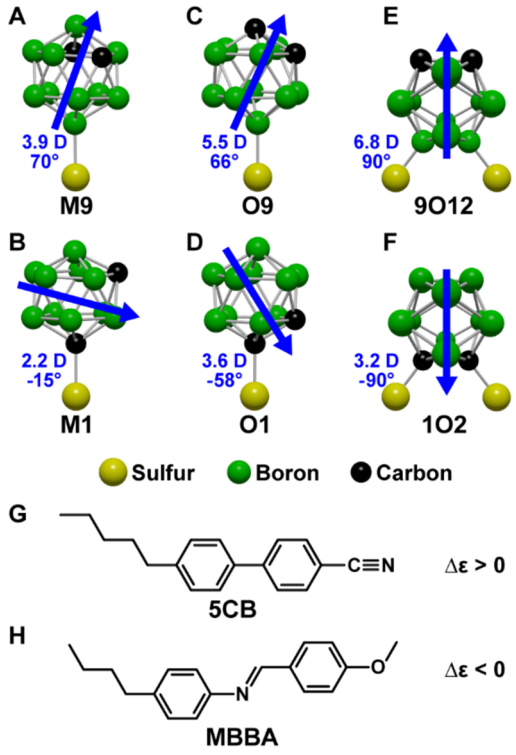

Figure 1. Molecular structures of carboranethiol and -dithiol isomers: (A) *m*-9-carboranethiol (**M9**), (B) *m*-1-carboranethiol (**M1**), (C) *o*-9-carboranethiol (**O9**), (D) *o*-1-carboranethiol (**O1**), (E) *o*-9,12-carboranedithiol (**9O12**), and (F) *o*-1,2-carboranedithiol (**1O2**). Dipole moment magnitudes and orientations, calculated for isolated molecules, are indicated in blue. Positive (negative) angles estimate dipole orientations above (below) the plane of the substrate when assembled onto gold surfaces. Mesogen molecular structures of (G) 4-cyano-4′-pentylbiphenyl (**5CB**) and (H) *N*-(4-methoxybenzylidene)-4-butylaniline (**MBBA**) with corresponding dielectric anisotropy ($\Delta\varepsilon$) signs noted. Hydrogen atoms are omitted from all structures for clarity.

To monitor SAM-regulated mesogen alignment, LC cells were constructed as shown in Figure 2A. The outgoing polarization of light transmitted through a cell depends on the angle between the polarization of the incoming light and the orientation of the nematic director, which represents the average alignment direction of mesogens in a LC. If the mesogens align homeotropically, this angle is independent of cell rotations about axes normal to the alignment layers and the cells appear "dark" (0% transmittance) when viewed between crossed polarizers. Variations in the intensity of transmitted light with rotations of the cell, however, indicate planar alignment of the nematic director. Figure 3 shows the modulation in the intensity of the light transmitted through **5CB** cells as they were rotated between crossed polarizers (Figure 2B); corresponding **MBBA** data are provided in the Supporting Information. Alignment layers treated with **M9**, **M1**, **O9**, **O1**, **9O12**, and **1O2** SAMs all induced uniaxial planar alignment in both **5CB** and **MBBA** cells, as indicated by the four-fold symmetry of their transmittance spectra. Cells constructed without a twist in their nematic directors vary

DOI: 10.1021/jacs.6b02026
J. Am. Chem. Soc. 2016, 138, 5957−5967

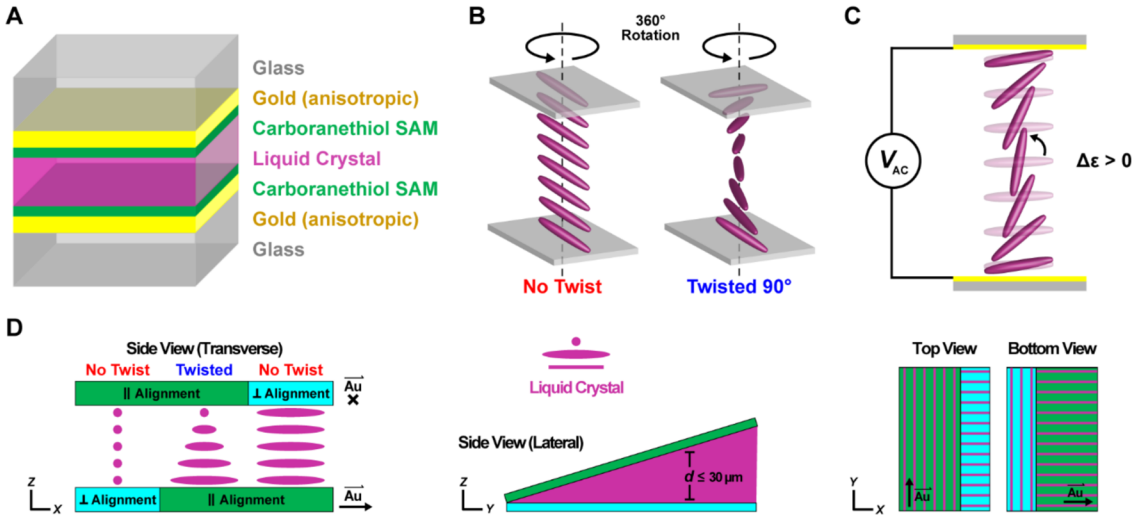

Figure 2. (A) Schematic of liquid crystal (LC) cells used in rotation and electrically modulated optical transmittance measurements ("transmittance cells"). Carboranethiol and -dithiol self-assembled monolayers (SAMs) adsorbed on semitransparent, anisotropic gold films induced uniaxial planar alignment of a LC at the interface. Schematics illustrating the rotation of LC cells 360° about axes normal to their alignment planes (B) and a Fréedericksz transition (C) in a LC with positive dielectric anisotropy ($\Delta\varepsilon > 0$) upon application of an alternating electric potential (V_{AC}). (D) Wedge cell geometry used to measure azimuthal anchoring energies, as viewed from multiple perspectives ("anchoring energy cells"). Each alignment layer was divided into two distinct sections defined by SAMs composed of complementary molecules. Here, a carboranethiol or -dithiol isomer SAM (green) is shown to induce LC alignment parallel to the gold deposition direction ($\vec{\mathbf{Au}}$), although other isomers may instead promote planar alignment perpendicular to $\vec{\mathbf{Au}}$. Alkanethiol SAMs (blue) were used to induce planar LC alignment orthogonal to that induced by the carboranethiol or -dithiol isomer. Once assembled, the cell was comprised of three nematic regions, one possessing a ~90° twist in the azimuthal director orientation, while the other two exhibited untwisted LC alignment (90° apart) through the bulk of the cell. The thickness (d) of the gap between the alignment layers varied due to the presence of a spacer (not shown) at only one end of the cell.

from nearly extinguishing all transmitted light to transmitting ~50%. By contrast, cells that possess a 90° twist in their directors have transmittances varying from ~50% to nearly 100%, due to the rotation of the transmitted light's polarization as it traverses the cell.[74]

Applying a potential difference between the alignment layers generates an electric field that can distort the planar alignment of LCs with $\Delta\varepsilon > 0$, inducing them to adopt an orientation parallel to the field (normal to the surface), as illustrated in Figure 2C.[75] This reorientation of the mesogens alters the transmittances of LC cells viewed between crossed polarizers, as shown in Figure 4. Transmittances of twisted nematic cells containing **5CB** ($\Delta\varepsilon > 0$) decrease to near 0% with increasing field strengths. By contrast, twisted nematic cells made using **MBBA** do not exhibit a change in their transmittance due to their $\Delta\varepsilon < 0$, maintaining planar alignments that are reinforced by the applied field (see Supporting Information). The applied potentials produce no lasting changes to the carboranethiol monolayers, as evidenced by the reproducibility of the voltage-modulated transmittance curves through repeated sweeping of the potential's amplitude between 0 and 7 V. The observed optical responses of the cells to applied electric fields is further indication of the planar alignment adopted by both **5CB** and **MBBA** LCs on carboranethiol and -dithiol SAMs.

The rotation- and field-induced variations in transmittance described above were observed uniformly over the entire area (~1 cm^2) of each cell measured. These results indicate uniaxial planar alignment of **5CB** and **MBBA** on anisotropic gold surfaces treated with each of the six carboranethiols considered here. However, these observations, alone, do not uniquely determine the nematic director orientation on a surface. Transmittance minima of untwisted nematics are expected when the director aligns along either of the crossed polarizers' axes, while maxima are expected at these orientations for cells constructed with 90° twists in their directors. These expectations are realized in Figure 3; transmittance extrema coincide with cell rotations that align $\vec{\mathbf{Au}}$ parallel to, and 45° from, the polarizers' axes. Two possible in-plane director orientations can produce this effect: director alignment parallel or perpendicular to $\vec{\mathbf{Au}}$.

In order to determine, unambiguously, the LC orientation relative to the gold deposition axis (parallel or perpendicular), a wedge cell geometry was used, as illustrated in Figure 5. Illuminating a LC wedge with monochromatic light, polarized 45° from its optical axis, produced a series of bright and dark fringes visible within the cell when observed between crossed polarizers. These fringes result from changes in the transmitted light's polarization as it traverses the birefringent cell. The optical retardation (Γ) between ordinary and extraordinary waves causes transmitted light to vary continuously between linear and elliptical polarization states, dependent on the wedge thickness (d). In the two extremes, light exits the wedge linearly polarized parallel or perpendicular to its incoming polarization, producing transmittance minima and maxima, respectively. The conditions on the optical retardation (wedge thickness) required for a transmittance extreme are given by

$$\Gamma = \Delta n d = \begin{cases} (m + {}^{1}/_{2})\lambda, & \text{maxima} \\ m\lambda, & \text{minima} \end{cases} \qquad m = 0, 1, 2, 3, \ldots \tag{1}$$

where λ is the wavelength of light, Δn is the LC's birefringence, and m is an integer enumerating the fringe order. Wave plates, inserted in series with a wedge cell between crossed polarizers, modify the total retardation by fixed amounts and cause the

DOI: 10.1021/jacs.6b02026
J. Am. Chem. Soc. 2016, 138, 5957−5967

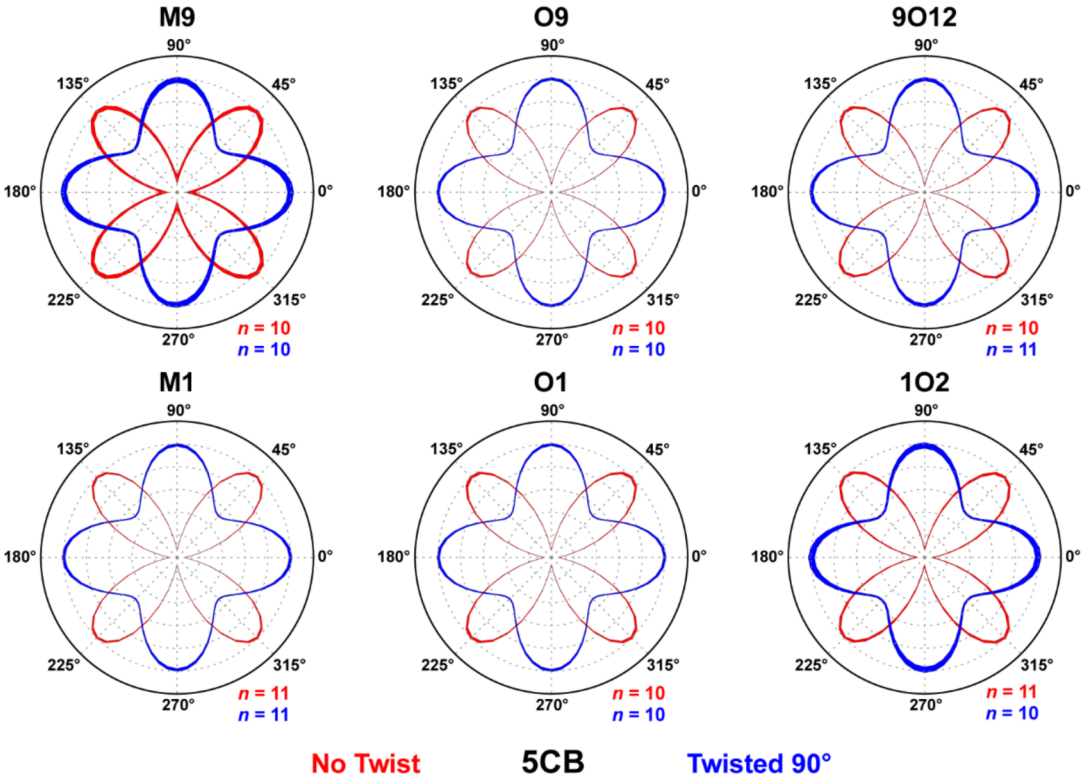

Figure 3. Optical transmittances (indicated by the radial distance from the origin, in arbitrary units) of liquid crystal (LC) cells rotated between crossed polarizers. Alignment layers were prepared with matching self-assembled monolayers of *m*-9-carboranethiol (**M9**), *m*-1-carboranethiol (**M1**), *o*-9-carboranethiol (**O9**), *o*-1-carboranethiol (**O1**), *o*-9,12-carboranedithiol (**9O12**), and *o*-1,2-carboranedithiol (**1O2**), as indicated. At these surfaces, uniaxial, planar alignment was manifest in 4-cyano-4′-pentylbiphenyl (**5BC**) LCs, as evidenced by the variations in optical transmittance possessing four-fold rotational symmetry. Cells were constructed with angles of either 0° or 90° between the alignment layers' gold deposition axes, inducing untwisted (red) or twisted (blue) nematic structures, respectively. Initially, one or both of a cell's gold deposition axes were aligned with the polarizer axis, defined to be at 0°. Rotation angles were measured with respect to this reference orientation, incremented in 5° steps. Reported spectra are averages of analyses performed on *n* separate LC cells, each consisting of three measured regions, where the radial line widths indicate the data's standard deviations. Spectra are scaled such that their respective transmittance maxima are equal; in actuality, the maximum transmittance of an untwisted nematic cell nearly equals the minimum transmittance of a cell with a 90° twist in its director.

apparent positions of the fringes to shift. When the optical axes of a wave plate and untwisted nematic align, the total retardation of the transmitted light increases, whereas when their optical axes are crossed, the retardation decreases. Increased (decreased) optical retardation results in shifts in the fringe position toward (away from) the vertex of the wedge, toward the thinner (thicker) end of the cell. In this way, one can infer the orientation of the nematic director from the known orientation of a wave plate's slow axis and the direction of the observed shift in fringe positions.

As shown in Figure 6, the fringes observed in cells made using **M1**, **O1**, and **1O2** SAMs shift toward the thinner ends of the cells with increased optical retardation along $\vec{\mathbf{Au}}$. This result indicates that the **5CB** director is aligned parallel to $\vec{\mathbf{Au}}$ in these cells. By contrast, cells prepared with **M9**, **O9**, and **9O12** SAMs induced planar alignment of the **5CB** director perpendicular to $\vec{\mathbf{Au}}$, as the fringes were observed to move toward the thicker ends of the cells. We note that self-assembled carboranethiol and -dithiol isomers with dipole moments directed toward the gold surface induced **5CB** alignment parallel to $\vec{\mathbf{Au}}$, whereas isomers with dipoles directed away from the substrate induced planar alignment perpendicular to $\vec{\mathbf{Au}}$. A similar tendency was also observed in the case of **MBBA** LCs (see Supporting Information), with the exceptions of **M9** and **1O2** SAMs, *vide infra*. Comparing the in-plane alignment orientations of **5CB** and **MBBA** directors enables us to examine and to constrain the coupling mechanism between the mesogens and carboranethiol SAMs. If a dipolar electric field due to the SAM dominates the interaction, then orthogonal director orientations of the two LCs (with oppositely signed values of $\Delta\varepsilon$) are expected. However, this behavior is *not* observed, which is understandable due to the inversion symmetry of the nematic director ($\vec{\eta}$ and $-\vec{\eta}$ represent equivalent director orientations).[76] Therefore, the molecular dipole moments in the SAM must influence mesogen alignment by other means.

Anchoring energy measures the work (per unit area) required to reorient a LC director perpendicular to its preferred, "easy axis" orientation on a surface. We compare azimuthal anchoring energies of **5CB** aligned by **M1**, **O9**, **O1**, and **9O12** monolayers as a means of quantifying SAM-LC interactions. In doing so, we test for differences in anchoring strengths between isomers that align LCs in the same, and perpendicular, directions on anisotropic gold surfaces. A torque-balance measurement scheme[77,78] was adopted to estimate anchoring energies on patterned, hybrid, alignment layers assembled in a wedge configuration, as illustrated in Figure 2D. Twisted and untwisted nematic regions in a cell were created using bifunctional alignment layers, pairing carboranethiol SAMs with alkanethiol monolayers known to

DOI: 10.1021/jacs.6b02026
J. Am. Chem. Soc. 2016, 138, 5957−5967

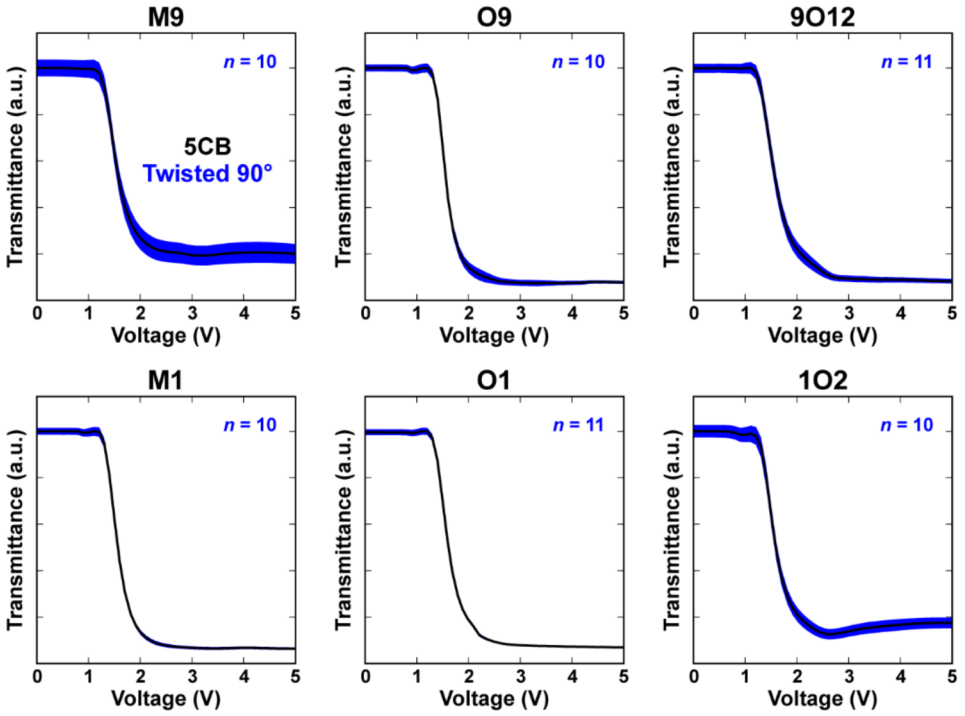

Figure 4. Normalized optical transmittances of electrically modulated liquid crystal (LC) cells viewed between crossed polarizers. Alignment layers were prepared with matching self-assembled monolayers of *m*-9-carboranethiol (**M9**), *m*-1-carboranethiol (**M1**), *o*-9-carboranethiol (**O9**), *o*-1-carboranethiol (**O1**), *o*-9,12-carboranedithiol (**9O12**), and *o*-1,2-carboranedithiol (**1O2**), as indicated. These surfaces induced uniaxial planar alignment in 4-cyano-4′-pentylbiphenyl (**5CB**) LCs. Cells were constructed with perpendicular gold deposition axes, producing twisted nematic structures, and were positioned between crossed polarizers such that their zero-voltage optical transmittance was maximized. Subsequently, a sinusoidally varying (1 kHz) voltage was applied between the alignment layers in order to distort the LC director away from the surface. Root-mean-square voltages, varied in 0.1 V steps, are indicated along the horizontal axes. Reported spectra are averages (black lines) of analyses performed on *n* separate LC cells, where the vertical widths of the surrounding blue outlines indicate the data's standard deviations.

induce planar LC alignment in orthogonal directions.[46] The untwisted nematic regions within the cells enable determination of the easy axes of both the top and bottom alignment layers, which coincide with the director orientation. In the twisted nematic regions, however, the director deviates from the surfaces' easy axes due to an elastic restoring torque acting on the mesogens as a result of the twist deformation through the bulk of the cell. The angle (φ) by which the director deviates from the easy axes, and thus partially untwists itself, is related to the azimuthal anchoring energy (W_{az}):

$$W_{az} = \frac{2K_{22}\Psi}{d\,\sin(2\varphi)} \qquad (2)$$

where K_{22} is the twist elastic constant of the mesogen and Ψ is the overall twist of the nematic director through a cell with thickness d (see Figure S5 in Supporting Information). In wedge cells, d varies continuously along their longitudinal axes and, as such, must be determined at each measurement location. Wedge thicknesses may be inferred from their apparent (transmitted) colors. When illuminated with white light and viewed between polarizers crossed at ±45° from the optical axis of an untwisted nematic with known birefringence, the color of transmitted light is related to a cell's thickness using a Michel−Lévy interference color chart.[79] However, this chart provides only a *qualitative* measure since it is based on a subjective judgment of color and is prone to misinterpretation. Monochromatic transmission fringes visible within a cell, like those seen in Figure 6, provided a *quantitative* means of estimating the wedge thickness using known values of Δn and λ in eq 1. In this way, we determined the **5CB** azimuthal anchoring energies summarized in Table 1.

If LC alignment is modulated by the monolayer's constituent dipole moments, we expect to observe differences in the anchoring strengths of alignment layers treated with different carboranethiol and -dithiol isomers. We found a nearly bimodal distribution of anchoring energies from the four carboranethiol SAMs tested here, with the stronger (weaker) anchoring surfaces corresponding to those with normal dipoles oriented toward (away from) the substrate. Anisotropic gold surfaces functionalized with either **O9** or **9O12** aligned **5CB** with approximately half the strength, perpendicular to $\overrightarrow{\mathbf{Au}}$, as monolayers of **M1** or **O1**, which induced alignment parallel to $\overrightarrow{\mathbf{Au}}$. Although each of these molecules possesses distinct dipole magnitudes and orientations, the anchoring strengths of **M1** and **O1** (both monothiol species) SAMs did not differ appreciably. By contrast, the anchoring energy measured on **9O12** (dithiol) SAMs was found to be ∼10% less than the value measured on **O9** (monothiol) SAMs. However, that decrease in anchoring energy coincides with a matching reduction in the areal density of **9O12** molecules within close-packed SAMs, compared with **O9** monolayers, due to the larger nearest-neighbor spacing of carboranedithiol adsorbates.[14,60,64] These findings suggest that the polarity of the normal dipole moment, toward or away from the surface, and the molecular packing density are the dominant factors affecting LC anchoring in these systems. We note that the measured anchoring energies of **5CB** LCs on carboranethiol monolayers (∼7 and ∼14 $\mu J \cdot m^{-2}$) exceed the values reported

DOI: 10.1021/jacs.6b02026
J. Am. Chem. Soc. 2016, 138, 5957−5967

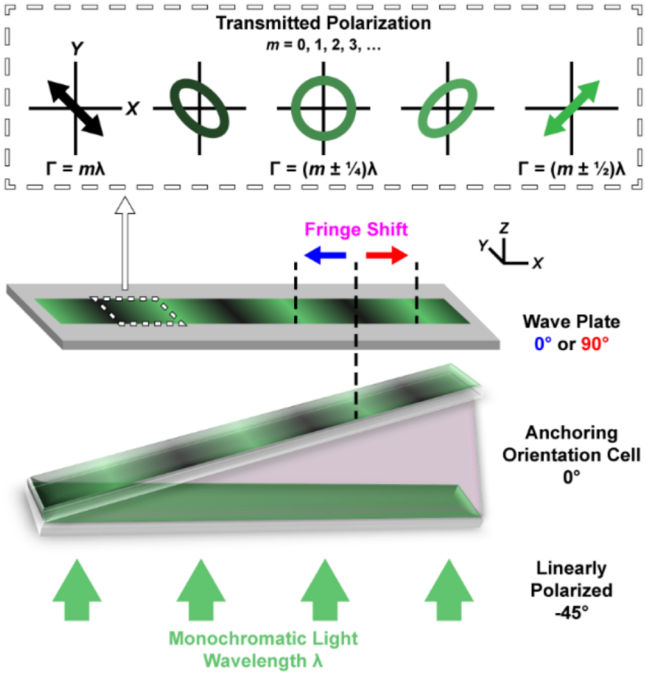

Figure 5. Wedge cell scheme used to determine the in-plane liquid crystal director orientation with respect to the alignment layers' gold deposition axes ("anchoring orientation cells"). Linearly polarized, monochromatic light (λ = 531 nm) traversing the cell accumulates an optical retardation (Γ) dependent on the wedge thickness. As a result, the transmitted light varies between linear and elliptical polarization states, as indicated along the top of the figure. This retardation is modified by placing wave plates in series with the cell. When the optical axes of the cell and wave plate align, the overall retardation increases, whereas when the optical axis of the wave plate is perpendicular to that of the nematic, the total retardation is reduced. When viewed through an analyzer (not shown), oriented 90° from the incoming light's polarization, a series of bright and dark fringes are visible within the cell due to extinction of light polarized along the initial direction. As shown, the wave plate modifies the optical retardation of the transmitted light by $\lambda/2$, thereby causing the transmittance maxima to become minima, and vice versa. All angles indicate orientations in the *xy*-plane with respect to the +*x*-axis.

for oligo(ethylene glycol)-containing SAMs (<6 μJ·m^{-2}),[78,80] and are comparable to those on unfunctionalized surfaces.[37,81,82] These values, however, are almost two orders of magnitude weaker than the anchoring strengths of rubbed polyamide films.[83,84]

Uncertainty in the local gold deposition angle is expected to be a major contributor to variations in the measured azimuthal anchoring energies.[38,80,85,86] All of the gold films used in these studies were deposited at the same angle, nominally 50° away from the surface normal. However, due to the finite sizes of the glass substrates and their positions relative to the evaporating metal source, departures of up to 6° from the intended angle are possible (see Supporting Information). Variations in the average grain size and surface roughness affect the substrate's contribution to LC alignment, resulting in stronger anchoring on gold films deposited at higher, more oblique angles.[85] Additionally, uncertainty in the anchoring energy typically increases with deposition angle due, in part, to its sensitivity to uncertainties in the nematic director's twist and deviation from the easy axes.[80] This sensitivity becomes more pronounced with increasing anchoring strength (higher deposition angles). The anchoring energies reported here reflect averages of

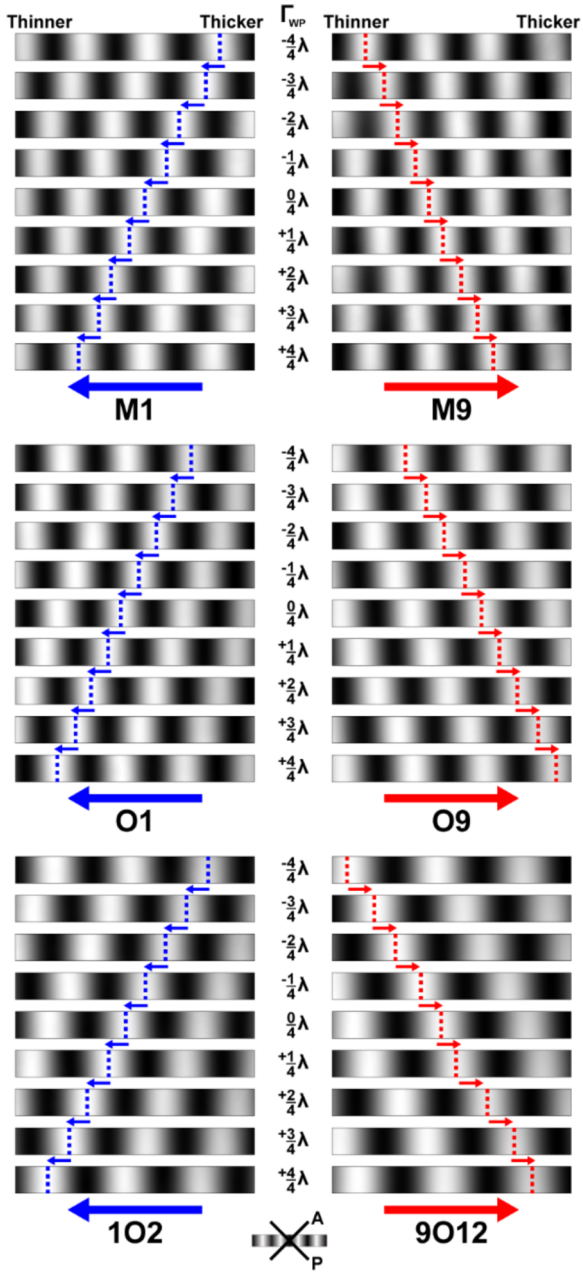

Figure 6. Transmission fringes observed in liquid crystal (LC) wedge cells viewed between crossed polarizers while illuminated with monochromatic light (wavelength λ = 531 nm). Alignment layers prepared with matching self-assembled monolayers of *m*-1-carboranethiol (**M1**), *m*-9-carboranethiol (**M9**), *o*-1-carboranethiol (**O1**), *o*-9-carboranethiol (**O9**), *o*-1,2-carboranedithiol (**1O2**), and *o*-9,12-carboranedithiol (**9O12**), as indicated, induced uniaxial planar alignment of 4-cyano-4′-pentylbiphenyl (**5CB**) LCs. Wave plates inserted between the polarizers modified the optical retardation of light transmitted through the cells by fixed amounts (Γ_{WP}). Here, positive (negative) values of Γ_{WP} signify that a wave plate's optically slow axis was aligned parallel (perpendicular) to a cell's gold deposition direction ($\vec{\mathbf{Au}}$). Arrows and dashed lines track transmittance maxima of constant order within 4.8 mm × 0.5 mm fields of view. Fringes in cells containing **M1**, **O1**, and **1O2** monolayers were observed to shift toward the thinner ends of the wedges with increasing Γ_{WP} (blue), indicating that their nematic directors were oriented parallel to $\vec{\mathbf{Au}}$. By contrast, fringes shifted toward the thicker ends of cells containing **M9**, **O9**, and **9O12** monolayers (red), indicating director alignment perpendicular to $\vec{\mathbf{Au}}$.

DOI: 10.1021/jacs.6b02026
J. Am. Chem. Soc. 2016, 138, 5957−5967

Table 1. Anchoring Energy (W_{az}) of 5CB Liquid Crystals in Cells Prepared with Various Carboranethiol Self-Assembled Monolayers (SAMs)

anchoring SAM[a]	$p_\perp$[b]	W_{az} (μJ·m^{-2})	sample size, n
O9[c]	↑	7.5 ± 0.1	28
9O12[d]		6.7 ± 0.1	29
M1[e]	↓	14.3 ± 0.4	36
O1[f]		14.3 ± 0.4	37

[a]Carboranethiol or -dithiol isomer used to align 4-cyano-4′-pentylbiphenyl (**5CB**). [b]Normal dipole ($p_\perp$) orientation toward (↓) or away from (↑) the gold surface. [c]*o*-9-Carboranethiol. [d]*o*-9,12-Carboranedithiol. [e]*m*-1-Carboranethiol. [f]*o*-1-Carboranethiol.

measurements performed on multiple cells, inversely weighted by their estimated variances. Such averaging, however, biases the reported values in favor of lower anchoring energies that possess correspondingly smaller uncertainties. The complete data sets, as well as a discussion of the statistical methods used in our analysis, are provided in the Supporting Information.

As noted above, we observe a trend in the alignment of LCs by carboranethiol monolayers prepared on anisotropic gold surfaces that follows the polarity of the adsorbate's normal dipole moment. The constituent molecules of a SAM, in general, possess dipoles with components oriented parallel and normal to the functionalized surface. The cumulative effects of the in-plane molecular dipoles are diminished by their varying or disordered azimuthal orientations expected at room temperature.[14] Molecules may adsorb to the surface with random in-plane dipole orientations and, in the cases of **M9**, **M1**, **O9**, and **O1**, which possess only a single attachment to the substrate, rotate about their Au−S bonds. If long-range orientational order is present, the formation of differently polarized domains (including closure domains) would compensate for a net in-plane dipole over macroscopic scales. Additionally, image dipoles, formed through the redistribution of charge on the underlying gold substrate, would further attenuate the effects of in-plane molecular dipoles. Normal dipole moments, however, are not subject to these mitigating factors. Each carboranethiol in a single-species SAM adsorbs to the surface with the same polar orientation and, as such, enhances the net dipole moment normal to the surface. Carboranedithiol isomers (**9O12** and **1O2**) were included in these experiments due to their expected dipole orientations normal to the surface as a result of their bilateral molecular symmetry. Since these isomers bind to the substrate via two Au−S bonds, they are not free to rotate azimuthally. In principle, these isomers could tilt about the axis connecting their two adsorbed thiolate moieties, out of the plane normal to the gold substrate, resulting in a portion of their dipole moments orienting parallel to the surface. Nevertheless, we observe the same trend in **5CB** alignment induced by carboranedithiol isomers as in the cases of monothiol isomers, dependent upon the polarity of the normal dipole. As such, we conclude that the net in-plane dipole of a SAM is either compensated through one or more of the mechanisms mentioned above, or is a less significant contributor than the normal dipole when determining LC alignment.

In addition to the factors discussed above, other surface anisotropies may contribute to the existence of an easy alignment axis. One such contribution originates from an anisotropic electric susceptibility of the alignment surface. Obliquely deposited films are expected to have an anisotropic response to electric stimuli (e.g., from mesogen dipoles) due to their dune-like or columnar surface textures.[87,88] Molecular monolayers can modify this anisotropy, dependent on the adsorbate polarizabilities and orientations on the surface. To examine this effect, molecular polarizability tensors ($\boldsymbol{\alpha}$) were calculated using density functional theory for each of the six carboranethiol and -dithiol isomers considered here (see Supporting Information). To facilitate comparison, Cartesian coordinate bases were chosen for each molecule such that the bond(s) connecting the sulfur atom(s) to the carborane cage moiety coincided with (or symmetrically straddled) the z-axis. Additionally, one or both of the carbon atoms within the isomers were designated to lie along the x-axis, in the cases of **M1**, **O9**, **O1**, **9O12**, and **1O2**, and symmetrically about the x-axis in the case of **M9**. These coordinate bases closely coincided with the molecules' principal polarizability axes, such that the off-diagonal polarizability tensor elements (α_{ij}, $i \neq j$) were negligible (<1%) by comparison to the diagonal elements (α_{ii}). Considering upright adsorption, we found that the molecular polarizabilities of carboranethiols were nearly symmetric in the plane of the substrate ($\alpha_{xx} \approx \alpha_{yy}$), with variations of <2%. Larger in-plane variations in molecular polarizability were found for **9O12** and **1O2** (~10%), in part due to the lower (two-fold) rotational symmetry of carboranedithiols compared that of with monothiol isomers (five-fold). Symmetric adsorbate polarizabilities reduce the likelihood of anisotropic in-plane polarizations of a SAM inducing LC alignment on flat, isotropic surfaces. On textured surfaces, however, the local (microscopic) surface normal generally deviates from that of the average (macroscopic) plane of the substrate, effectively varying the orientations of molecules within the assembly. As a result, the in-plane electric susceptibility of a SAM depends, in part, on the polarizability of carboranethiols along their z-axes (α_{zz}), which is ~20% greater than their polarizability along orthogonal directions. Therefore, geometric surface anisotropies present in obliquely deposited films, generate additional anisotropies in a monolayer without requiring, *a priori*, long-range azimuthal alignment of carboranethiols. However, we do not find any consistent correlation between the observed LC alignment and all six of the carboranethiol molecular polarizabilities considered here.

Comparing the alignments of mesogens with oppositely signed dielectric anisotropies provides insight into the role of the dipolar field on LC anchoring by functionalized surfaces. Assuming direct coupling between the mesogens and the field, **5CB** and **MBBA** LCs were expected to align along orthogonal directions, relative to each other, at the SAM-LC interface. Instead, both mesogens adopted the same planar orientation, dependent on the polarity of the monolayer's constituent molecular dipoles normal to the surface, as detailed previously. However, in the case of **MBBA** alignment, **M9** and **1O2** carboranethiol monolayers were found to be exceptions to this trend. Alignment layers functionalized with **M9** induced alignment of **MBBA** parallel to $\vec{\mathbf{Au}}$, whereas **1O2** monolayers resulted in more heterogeneous and less reproducible anchoring of **MBBA** than observed on surfaces treated with other isomers under the same conditions. To understand these anomalies, we reemphasize that the monolayer's constituent dipoles are not the sole factor affecting LC alignment, despite being the focus of these studies. Other influences, including surface topography, molecular geometry, tilt, and order, are still present (albeit consistent) in each cell, while the contribution

DOI: 10.1021/jacs.6b02026
J. Am. Chem. Soc. 2016, 138, 5957−5967

from carboranethiol dipoles varies between isomers. Out of the three isomers with dipoles directed away from the underlying gold surface tested here, **M9** possesses the weakest moment and is the only one to induce LC alignment counter to the prevailing trend (and only with **MBBA**). Previously, we noted that the anchoring strength of **5CB** on carborane-functionalized surfaces did not depend on the magnitude of the molecular dipoles of a SAM. This unexpected alignment of **MBBA** may indicate a minimum threshold strength of molecular dipoles required to orient LCs along a particular direction on these surfaces. Alternatively, we propose that the properties of **MBBA** itself may instead be responsible. Relative to **5CB**, **MBBA** has a weaker internal dipole moment and smaller dielectric anisotropy (see Supporting Information). As a result, the coupling strength of **MBBA** to external electric fields is weaker than that of **5CB**, with which no alignment anomalies were observed. Future experiments using a LC with a more negative dielectric anisotropy could test this hypothesis and distinguish whether or not the observed alignment is indicative of the carboranethiol monolayer or a property of the mesogen itself. In the case of the heterogeneous alignment of **MBBA** on **1O2** monolayers, we note the potential for dithiol isomers to chemisorb to the gold surface in either singly or doubly bound states. Here, we used ethanolic solutions of each of the carboranedithiols with added base (sodium hydroxide) to promote dual binding via both thiol moieties on each molecule. However, even under these circumstances, not every adsorbed molecule binds to the gold with both thiol moieties. We have observed elsewhere[64] that the **1O2** isomer is more likely to adsorb in mixed states (both singly and doubly bound) compared to the **9O12** isomer under alkaline conditions, resulting in a less uniform SAM. This molecular-scale heterogeneity may, in turn, produce more heterogeneous LC arrangements than those observed on alignment layers treated with other carboranethiol isomers.

■ CONCLUSION AND PROSPECTS

Here, LCs serve as advantageous probes of the nanoscale intermolecular forces between SAMs and their environment. These combinations of forces result from several factors, including surface topography, molecular orientation, and chemical functionality, which modulate the properties of the underlying substrate and mediate the assembly of adsorbates. We report on the uniaxial, planar alignment of **5CB** and **MBBA** LCs on obliquely deposited gold films functionalized with carboranethiol and -dithiol SAMs. Carboranethiol monolayers enable direct comparisons of LC alignment modulated by differences in the magnitudes and orientations of assembled molecular dipoles on a surface. Carboranethiol monolayers hold *constant* other factors that influence LC alignment, such as molecular geometry, tilt, and order, which have confounded previous studies. Furthermore, comparing LC alignment on monolayers composed of monothiol isomers (**M9**, **M1**, **O9**, and **O1**) to those composed of carboranedithiols (**9O12** and **1O2**) enabled inference of the roles of the normal and lateral surface dipoles. We observed that the in-plane, azimuthal orientation of mesogens on anisotropic gold films was modulated predominantly by the carboranethiol dipole component normal to the surface. Monolayers composed of carboranethiols with dipoles oriented toward (away from) the underlying gold surface induced planar alignment of **5CB** parallel (perpendicular) to the gold deposition direction. A similar trend was observed in the case of alignment of **MBBA**, which possesses an oppositely signed dielectric anisotropy. Since LCs with dielectric anisotropies of opposite signs align similarly, dependent on the monolayer's normal dipole polarity, we conclude that it is not a direct result of dipolar field coupling between SAMs and mesogens. We attribute the observed alignment to more complex mechanisms involving intermolecular dispersion forces. To quantify SAM-LC interaction strength, we measured the azimuthal anchoring energies of **5CB** on alignment layers treated with **M1**, **O9**, **O1**, and **9O12** monolayers. A nearly bimodal distribution of anchoring energies was measured, dependent on the polarity of the carboranethiol isomer dipole moment component normal to the surface. Monolayers composed of carboranethiol isomers with dipoles oriented away from (**O9** and **9O12**) and toward (**M1** and **O1**) the substrate were measured to anchor **5CB** with strengths of ∼7 and ∼14 $\mu J \cdot m^{-2}$, respectively. Additionally, comparing the anchoring energies of pairs of isomers with the same polarity normal to the surface, we found no difference in anchoring strengths between monothiol species (**M1** and **O1**). However, we observed that the anchoring energies measured on surfaces treated with **9O12** (dithiol) were about 10% lower than those measured on surfaces treated of **O9** (monothiol), coinciding with the decrease in areal density of carboranethiols within the close-packed monolayers. This result indicates that not only the polarities of the molecular dipoles affect LC anchoring, but also their densities on the surfaces. We also considered other sources of surface anisotropy arising from the molecular polarizabilities of the carboranethiols used in this work that may affect LC anchoring direction and strength. We do not expect that long-range molecular alignment of carboranethiol adsorbates within SAMs at room temperature is likely.[14] However, others have previously observed azimuthal ordering of exposed methyl moieties in alkanethiol monolayers prepared on anisotropic gold films.[41] Complementary techniques, such as sum-frequency generation spectroscopy, may be used in future studies to test this possibility in the case of carboranethiol SAMs.[89] The mechanism involved remain unresolved, but this work isolates elements of the alignment of LCs on functionalized, anisotropic surfaces in order to elucidate the role of molecular dipole moments of the monolayers on the subsequent adsorption and assembly of other molecular species. Extending this knowledge to other molecular systems will enhance the predictive capabilities of nanoscale engineering and enable rational design of structures extended to macroscopic scales on complex surfaces.

■ EXPERIMENTAL SECTION

Materials. Positional isomers of dicarba-*closo*-dodecaboranethiol and -dithiol **O1**, **O9**, **1O2**, and **9O12** were synthesized using previously reported methods;[90−92] **M1** and **M9** isomers were purchased from Sigma-Aldrich (St. Louis, MO). Mesogens **5CB** and **MBBA**, as well as sodium hydroxide, and alkanethiols 1-undecanethiol (**C11**) and 1-octadecanethiol (**C18**) were also obtained from Sigma-Aldrich. Ethanol (200 proof) was purchased from Goldshield Chemical Company (Hayward, CA), while potassium hydroxide and hydrogen peroxide (30%) were acquired from Fisher Scientific (Pittsburgh, PA). Sulfuric acid (98%) was purchased from EMD Chemicals (Gibbstown, NJ). All commercial chemicals were used as received. Deionized (DI) water (18.2 MΩ·cm) was dispensed from a Milli-Q water purifier (EMD Millipore, Billerica, MA).

Polymeric Stamp Preparation. Polymeric stamps were produced using a Sylgard 184 silicone elastomer kit (Dow Corning, Midland, MI) following a previously reported procedure.[93] Flat, featureless

DOI: 10.1021/jacs.6b02026
J. Am. Chem. Soc. 2016, 138, 5957−5967

stamps were obtained and cut into strips approximately 8 mm wide, 76 mm long, and 4 mm thick.

Polarizing Microscopy and Image Analysis. An Olympus BX51-P polarizing microscope and CCD camera (Center Valley, PA) were used throughout this work to record the transmittances and optical textures of LC cells as 8-bit grayscale images. The transmittance of a LC cell was computed using the average intensity of all pixels within an image (1600 × 1200 pixels). Variations in the transmittance within the microscope field of view were quantified using the standard deviation of pixel intensities. Reported transmittance values reflect aggregated analyses of multiple cells and multiple locations within each cell. Automated routines facilitated image processing.

Alignment Layer Preparation. Eagle XG glass (Corning Display Technologies, Corning, NY), 1.1 mm thick, was used throughout this work. Glass used in anchoring energy measurements had lateral dimensions of 76 mm × 25 mm, while pieces intended for transmittance measurements were cut to approximately 19 mm × 25 mm.

Substrate Cleaning. Glass substrates were cleaned through sequential rinsing and ultrasonication steps (>20 min) in ethanol, DI water, and concentrated potassium hydroxide solution. Afterward, the glass was rinsed in DI water and then immersed in piranha solution (3:1 H_2SO_4/H_2O_2) for ∼1 h before a final rinse in DI water and being blown dry with nitrogen gas.

Oblique Metal Deposition. Cleaned glass substrates were loaded into the vacuum chamber of an electron beam metal evaporator (Kurt J. Lesker Company, Jefferson Hills, PA) immediately after drying and held at a base pressure of $\sim 1 \times 10^{-7}$ Torr. The substrates were mounted with fixed positions and orientations within the chamber such that their surface normal was inclined at an angle of 50° away from the metal source. Semitransparent gold films (10 nm) were deposited on top of chromium adhesion layers (2 nm) at rates of ∼0.5 Å/s. Nominal film thicknesses were measured using a quartz crystal microbalance orientated toward the metal source, thus overestimating the amount of metal adsorbed on the glass by a factor of sec(50°) ≈ 1.6. Due to the finite sizes of the glass substrates and their positions relative to the metal source, a deviation of <6° from the intended deposition angle is expected for gold films deposited in the same batch.

Self-Assembled Monolayer Preparation. Self-assembled monolayers were formed on obliquely deposited Au/glass substrates from 1 mM ethanolic solutions of the desired adsorbate: **O1**, **O9**, **M1**, **M9**, **1O2**, **9O12**, **C11**, or **C18**. In the cases of **1O2** and **9O12**, 1:2 carboranedithiol/NaOH equivalent solutions in ethanol were used to promote divalent adsorption on the gold surface.[64] Immediately prior to SAM deposition, Au/glass substrates were exposed to an oxygen plasma (Harrick Plasma, Ithaca, NY) for 40 s in order to remove adventitious organic adsorbates. Substrates intended for use in transmittance measurements were immersed in solutions of the desired carboranethiol or -dithiol isomer for 12−18 h. Afterward, the uniformly functionalized surfaces were rinsed in copious amounts of ethanol and then blown dry with nitrogen gas. By contrast, soft lithography was employed to create two adjacent, spatially separated, SAMs on substrates used in anchoring energy measurements. A polymeric stamp was soaked in a solution of either **C11** or **C18** "ink" for at least 20 min, then rinsed with ethanol and blown dry with nitrogen gas. The inked stamp was placed into conformal contact with a clean Au/glass surface for 10 min. This stamping resulted in the formation of an alkanethiol SAM over about one-third of the alignment surface (conformal contact area). The surface was then immersed into a solution of the carboranethiol or -dithiol under investigation for 60 min in order to functionalize the remaining bare surface. Finally, the surface was rinsed with ethanol and blown dry with nitrogen gas. Observing the distinct wetting behavior of ethanol over the two SAM regions, possessing either nonpolar (aliphatic) or polar (carborane) moieties, confirmed the bifunctional character of the surface.

Liquid Crystal Cell Assembly. All LC cells were assembled (*vide infra*) immediately following alignment layer preparation and their cavities filled with either **5CB** or **MBBA** via capillary action. To prevent flow-induced LC alignment, the alignment layers and mesogens were heated to 5−10 °C above the mesogen's clearing temperature during filling. Afterward, the cells were allowed to cool to room temperature (∼20 °C) and permanently sealed using cyanoacrylate adhesive (Henkel, Westlake, OH).

Transmittance Cells. Transmittance cells were assembled using plastic spacers (30 μm thick) to separate the matching functionalized gold surfaces of two alignment layers. Alignment layers were paired such that their gold deposition axes were either parallel or crossed at angles of ∼90°, producing cells with untwisted or twisted nematic structures, respectively. Copper wires were affixed to the outermost edges of both gold surfaces using conductive carbon glue (Ted Pella, Redding, CA), enabling manipulation of LC orientations by applied electric fields (potentials).

Anchoring Orientation Cells. The alignment layers of cells used to determine the in-plane LC anchoring orientations were prepared identically to those used in transmittance measurements. However, in contrast to transmittance cells, anchoring orientation cells were constructed as wedges with a spacer separating the alignment layers at only one end. In this configuration, the thickness of the cavity between the alignment layers varied linearly along the cell's longitudinal axis, independent of the transverse position. Only untwisted nematic cells, with parallel anisotropy axes, were used to determine anchoring orientations.

Anchoring Energy Cells. Adopting the design described by Abbott and co-workers,[77,78] anchoring energy cells were constructed with the wedge cell geometry described previously and engineered to contain three nematic regions. Alignment layers were arranged with crossed gold deposition axes, oriented along the longitudinal and transverse cell axes, and with matched and mismatched overlapping SAM regions, as illustrated in Figure 2D. As such, the azimuthal director orientation was induced to twist by ∼90° in the central region, whereas the regions on either side exhibited untwisted, uniaxial LC alignment (90° apart) through the bulk of the cell. To prevent flexing of the alignment layers during assembly, custom-built jigs were used to ensure uniform compression. Flexing was not observed to pose a problem when constructing other, comparatively shorter, types of LC cells.

Transmittance Measurements. Transmittance cells were examined between the crossed polarizers of a polarizing optical microscope while illuminated with white light. The optical axes of the cells were aligned initially with either of the microscope's polarizing axes, thus minimizing (maximizing) the relative intensity of light transmitted through cells constructed with no twist (90° twist) in their nematic directors. The transmittance was measured at 5° intervals over one complete rotation of a cell. This process was repeated three times, in different regions (1.2 mm × 0.9 mm field of view), for each cell measured. Afterward, the orientation of the cell was fixed and its transmittance measured as a sinusoidally varying voltage was applied between the alignment layers (3.0 mm × 2.2 mm field of view).

Anchoring Orientation Determination. Anchoring orientation cells were illuminated with monochromatic light polarized 45° from their optical axes. When viewed through an analyzer crossed 90° from the polarization of the incoming light, a series of bright and dark fringes were observed, as illustrated in Figure 5. These fringes were a consequence of differences in the optical retardation of light transmitted through the birefringent, LC, wedges. Wave plates (RealD, Beverly Hills, CA, and Edmund Optics, Barrington, NJ) were inserted between the polarizers, in series with the cells, to alter this retardation by fixed amounts. Changes in the fringe positions due to the wave plates were tracked within viewing areas of about 6.0 mm × 4.5 mm.

Anchoring Energy Measurements. Azimuthal anchoring energies were measured using a similar procedure to that reported by Abbott and co-workers.[78] The LC alignment directions and twist angles were determined using automated routines to fit the observed rotation−transmittance spectra in each of the cells' three nematic regions (590 μm × 440 μm field of view) to their expected trigonometric responses. Estimates of local wedge cavity thicknesses were made by comparing the observed color of cells illuminated with

DOI: 10.1021/jacs.6b02026
J. Am. Chem. Soc. 2016, 138, 5957−5967

white light to a Michel–Lévy interference color chart.[79] These estimates were refined using the positions of the transmission fringes made visible by illuminating the cells with monochromatic light. Transmittance minima and maxima bands acted as internal graduations corresponding to known cavity thicknesses. Reported anchoring energies represent an average of all measurements weighted by their respective measurement uncertainties (see Supporting Information).

Density Functional Theory Calculations. The six carboranethiol isomers used in this work were analyzed using density functional theory. Optimized molecular structures, dipole moments, and polarizabilities were computed at the M062X level of theory using the 6-311G** basis set with the Gaussian 09 software package (Gaussian, Wallingford, CT).[94,95]

■ ASSOCIATED CONTENT

Supporting Information

The Supporting Information is available free of charge on the ACS Publications website at DOI: 10.1021/jacs.6b02026.

Physical properties of **5CB** and **MBBA** LCs; rotation- and voltage-induced transmittance variations of **MBBA** LC cells; in-plane director orientations of **MBBA** LC cells; voltage-induced transmittance variations of untwisted nematic **5CB** LC cells; discussions of anchoring energy measurements and analysis (including complete data set); details concerning oblique gold deposition; results of density functional theory analysis (PDF)

■ AUTHOR INFORMATION

Corresponding Authors

*psw@cnsi.ucla.edu
*spokoyny@chem.ucla.edu
*chadnano@northwestern.edu
*tbase@iic.cas.cz

Notes

The authors declare no competing financial interest.

■ ACKNOWLEDGMENTS

The authors thank Dr. Rosario Esposito, Dr. Frank Kyte, and Shylo Stiteler for their assistance in this work and Prof. Nick Abbott for helpful discussions. We acknowledge financial support from the U.S. Department of Energy (grant no. DE-SC-0005025) for support of these experiments and their analysis, the National Science Foundation (grant no. DGE-1144087) for a graduate fellowship for A.M.M., and the Royal Thai Government for a graduate fellowship for N.W. A.M.S. thanks UCLA for start-up funds. C.A.M. acknowledges support by the following grants: National Science Foundation CHE-1149314 and U.S. Army W911NF-11-1-0229.

■ REFERENCES

(1) Whitesides, G. M.; Grzybowski, B. *Science* **2002**, *295*, 2418–2421.
(2) Smith, R. K.; Lewis, P. A.; Weiss, P. S. *Prog. Surf. Sci.* **2004**, *75*, 1–68.
(3) Love, J. C.; Estroff, L. A.; Kriebel, J. K.; Nuzzo, R. G.; Whitesides, G. M. *Chem. Rev.* **2005**, *105*, 1103–1170.
(4) Claridge, S. A.; Liao, W.-S.; Thomas, J. C.; Zhao, Y.; Cao, H. H.; Cheunkar, S.; Serino, A. C.; Andrews, A. M.; Weiss, P. S. *Chem. Soc. Rev.* **2013**, *42*, 2725–2745.
(5) Fersht, A. R.; Matouschek, A.; Serrano, L. *J. Mol. Biol.* **1992**, *224*, 771–782.
(6) Kudernac, T.; Lei, S.; Elemans, J. A. A. W.; De Feyter, S. *Chem. Soc. Rev.* **2009**, *38*, 402–421.
(7) Grzelczak, M.; Vermant, J.; Furst, E. M.; Liz-Marzán, L. M. *ACS Nano* **2010**, *4*, 3591–3605.
(8) Israelachvili, J. N. *Intermolecular and Surface Forces*, 3rd ed.; Israelachvili, J. N., Ed.; Academic Press: San Diego, 2011.
(9) Lee, H. J.; Jamison, A. C.; Lee, T. R. *Acc. Chem. Res.* **2015**, *48*, 3007–3015.
(10) Paniagua, S. A.; Hotchkiss, P. J.; Jones, S. C.; Marder, S. R.; Mudalige, A.; Marrikar, F. S.; Pemberton, J. E.; Armstrong, N. R. *J. Phys. Chem. C* **2008**, *112*, 7809–7817.
(11) Bishop, K. J. M.; Wilmer, C. E.; Soh, S.; Grzybowski, B. A. *Small* **2009**, *5*, 1600–1630.
(12) Liang, H.; Sun, W.; Jin, X.; Li, H.; Li, J.; Hu, X.; Teo, B. K.; Wu, K. *Angew. Chem., Int. Ed.* **2011**, *50*, 7562–7566.
(13) Kim, J.; Rim, Y. S.; Liu, Y.; Serino, A. C.; Thomas, J. C.; Chen, H.; Yang, Y.; Weiss, P. S. *Nano Lett.* **2014**, *14*, 2946–2951.
(14) Thomas, J. C.; Schwartz, J. J.; Hohman, J. N.; Claridge, S. A.; Auluck, H. S.; Serino, A. C.; Spokoyny, A. M.; Tran, G.; Kelly, K. F.; Mirkin, C. A.; Gilles, J.; Osher, S. J.; Weiss, P. S. *ACS Nano* **2015**, *9*, 4734–4742.
(15) Kulkarni, C.; Bejagam, K. K.; Senanayak, S. P.; Narayan, K. S.; Balasubramanian, S.; George, S. J. *J. Am. Chem. Soc.* **2015**, *137*, 3924–3932.
(16) Lewis, P. A.; Smith, R. K.; Kelly, K. F.; Bumm, L. A.; Reed, S. M.; Clegg, R. S.; Gunderson, J. D.; Hutchison, J. E.; Weiss, P. S. *J. Phys. Chem. B* **2001**, *105*, 10630–10636.
(17) Zhang, S. *Nat. Biotechnol.* **2003**, *21*, 1171–1178.
(18) Dameron, A. A.; Charles, L. F.; Weiss, P. S. *J. Am. Chem. Soc.* **2005**, *127*, 8697–8704.
(19) Barth, J. V.; Costantini, G.; Kern, K. *Nature* **2005**, *437*, 671–679.
(20) Aizenberg, J.; Black, A. J.; Whitesides, G. M. *J. Am. Chem. Soc.* **1999**, *121*, 4500–4509.
(21) Chen, S.; Liu, L.; Zhou, J.; Jiang, S. *Langmuir* **2003**, *19*, 2859–2864.
(22) Briseno, A. L.; Aizenberg, J.; Han, Y.-J.; Penkala, R. A.; Moon, H.; Lovinger, A. J.; Kloc, C.; Bao, Z. *J. Am. Chem. Soc.* **2005**, *127*, 12164–12165.
(23) Hermes, S.; Schröder, F.; Chelmowski, R.; Wöll, C.; Fischer, R. A. *J. Am. Chem. Soc.* **2005**, *127*, 13744–13745.
(24) Lee, C.-Y.; Gong, P.; Harbers, G. M.; Grainger, D. W.; Castner, D. G.; Gamble, L. J. *Anal. Chem.* **2006**, *78*, 3316–3325.
(25) Scherb, C.; Schödel, A.; Bein, T. *Angew. Chem.* **2008**, *120*, 5861–5863.
(26) Yao, Y.; Dong, H.; Hu, W. *Polym. Chem.* **2013**, *4*, 5197–5205.
(27) Palma, C.-A.; Cecchini, M.; Samorì, P. *Chem. Soc. Rev.* **2012**, *41*, 3713–3730.
(28) Roussel, T. J.; Barrena, E.; Ocal, C.; Faraudo, J. *Nanoscale* **2014**, *6*, 7991–8001.
(29) Meier, G.; Sackmann, E.; Grabmaier, J. G. *Applications of Liquid Crystals*; Springer-Verlag: Berlin, 1975.
(30) Gelbart, W. M. *J. Phys. Chem.* **1982**, *86*, 4298–4307.
(31) Jerome, B. *Rep. Prog. Phys.* **1991**, *54*, 391–452.
(32) Lee, K.-W.; Paek, S.-H.; Lien, A.; Durning, C.; Fukuro, H. *Macromolecules* **1996**, *29*, 8894–8899.
(33) Stöhr, J.; Samant, M. G. *J. Electron Spectrosc. Relat. Phenom.* **1999**, *98–99*, 189–207.
(34) Janning, J. L. *Appl. Phys. Lett.* **1972**, *21*, 173–174.
(35) Ichimura, K. *Chem. Rev.* **2000**, *100*, 1847–1874.
(36) O'Neill, M.; Kelly, S. M. *J. Phys. D: Appl. Phys.* **2000**, *33*, R67–R84.
(37) Skaife, J. J.; Abbott, N. L. *Chem. Mater.* **1999**, *11*, 612–623.
(38) Wilderbeek, H. T. A.; van der Meer, F. J. A.; Feldman, K.; Broer, D. J.; Bastiaansen, C. W. M. *Adv. Mater.* **2002**, *14*, 655–658.
(39) Berreman, D. W. *Phys. Rev. Lett.* **1972**, *28*, 1683–1686.
(40) Abelmann, L.; Lodder, C. *Thin Solid Films* **1997**, *305*, 1–21.
(41) Follonier, S.; Miller, W. J. W.; Abbott, N. L.; Knoesen, A. *Langmuir* **2003**, *19*, 10501–10509.
(42) Hoogboom, J.; Rasing, T.; Rowan, A. E.; Nolte, R. J. M. *J. Mater. Chem.* **2006**, *16*, 1305–1314.

DOI: 10.1021/jacs.6b02026
J. Am. Chem. Soc. 2016, 138, 5957–5967

(43) Drawhorn, R. A.; Abbott, N. L. *J. Phys. Chem.* **1995**, *99*, 16511−16515.
(44) Evans, S. D.; Allinson, H.; Boden, N.; Henderson, J. R. *Faraday Discuss.* **1996**, *104*, 37−48.
(45) Gupta, V. K.; Abbott, N. L. *Langmuir* **1996**, *12*, 2587−2593.
(46) Gupta, V. K.; Abbott, N. L. *Phys. Rev. E: Stat. Phys., Plasmas, Fluids, Relat. Interdiscip. Top.* **1996**, *54*, R4540−R4543.
(47) Gupta, V. K.; Abbott, N. L. *Science* **1997**, *276*, 1533−1536.
(48) Alkhairalla, B.; Allinson, H.; Boden, N.; Evans, S. D.; Henderson, J. R. *Phys. Rev. E: Stat. Phys., Plasmas, Fluids, Relat. Interdiscip. Top.* **1999**, *59*, 3033−3039.
(49) Carlton, R. J.; Hunter, J. T.; Miller, D. S.; Abbasi, R.; Mushenheim, P. C.; Tan, L. N.; Abbott, N. L. *Liq. Cryst. Rev.* **2013**, *1*, 29−51.
(50) Bramble, J. P.; Evans, S. D.; Henderson, J. R.; Anquetil, C.; Cleaver, D. J.; Smith, N. J. *Liq. Cryst.* **2007**, *34*, 1059−1069.
(51) Critchley, K.; Cheadle, E. M.; Zhang, H.-L.; Baldwin, K. J.; Liu, Q.; Cheng, Y.; Fukushima, H.; Tamaki, T.; Batchelder, D. N.; Bushby, R. J.; Evans, S. D. *J. Phys. Chem. B* **2009**, *113*, 15550−15557.
(52) Yoon, H.; Kang, S.-W.; Lehmann, M.; Park, J. O.; Srinivasarao, M.; Kumar, S. *Soft Matter* **2011**, *7*, 8770−8775.
(53) Crawford, G. P.; Ondris-Crawford, R. J.; Doane, J. W.; Žumer, S. *Phys. Rev. E: Stat. Phys., Plasmas, Fluids, Relat. Interdiscip. Top.* **1996**, *53*, 3647−3661.
(54) Tao, F.; Bernasek, S. L. *Chem. Rev.* **2007**, *107*, 1408−1453.
(55) Nakata, M.; Zanchetta, G.; Buscaglia, M.; Bellini, T.; Clark, N. A. *Langmuir* **2008**, *24*, 10390−10394.
(56) Bai, Y.; Abbott, N. L. *J. Am. Chem. Soc.* **2012**, *134*, 548−558.
(57) Bai, Y.; Abbasi, R.; Wang, C.; Abbott, N. L. *Angew. Chem., Int. Ed.* **2014**, *53*, 8079−8083.
(58) Grimes, R. N. *Carboranes*, 2nd ed..; Academic Press: Oxford, 2011.
(59) Kaszynski, P.; Douglass, A. G. *J. Organomet. Chem.* **1999**, *581*, 28−38.
(60) Hohman, J. N.; Zhang, P.; Morin, E. I.; Han, P.; Kim, M.; Kurland, A. R.; McClanahan, P. D.; Balema, V. P.; Weiss, P. S. *ACS Nano* **2009**, *3*, 527−536.
(61) Hohman, J. N.; Claridge, S. A.; Kim, M.; Weiss, P. S. *Mater. Sci. Eng., R* **2010**, *70*, 188−208.
(62) Cioran, A. M.; Musteti, A. D.; Teixidor, F.; Krpetić, Ž.; Prior, I. A.; He, Q.; Kiely, C. J.; Brust, M.; Viñas, C. *J. Am. Chem. Soc.* **2012**, *134*, 212−221.
(63) Kabytaev, K. Z.; Everett, T. A.; Safronov, A. V.; Sevryugina, Y. V.; Jalisatgi, S. S.; Hawthorne, M. F. *Eur. J. Inorg. Chem.* **2013**, *2013*, 2488−2491.
(64) Thomas, J. C.; Serino, A. C.; Goronzy, D. P.; Auluck, H. S.; Irving, O. R.; Deirmenjian, J. M.; Sautet, P.; Alexandrova, A. N.; Macháček, J.; Baše, T.; Weiss, P. S. Acid-Base Control of Valency within Carboranedithiol Self-Assembled Monolayers: Molecules Do the Can-Can. Manuscript in preparation.
(65) Kristiansen, K.; Stock, P.; Baimpos, T.; Raman, S.; Harada, J. K.; Israelachvili, J. N.; Valtiner, M. *ACS Nano* **2014**, *8*, 10870−10877.
(66) Dey, S.; Pal, A. J. *Langmuir* **2011**, *27*, 8687−8693.
(67) Brennan, T. P.; Tanskanen, J. T.; Bakke, J. R.; Nguyen, W. H.; Nordlund, D.; Toney, M. F.; McGehee, M. D.; Sellinger, A.; Bent, S. F. *Chem. Mater.* **2013**, *25*, 4354−4363.
(68) Breuer, T.; Witte, G. *ACS Appl. Mater. Interfaces* **2015**, *7*, 20485−20492.
(69) Pang, S. H.; Medlin, J. W. *J. Phys. Chem. Lett.* **2015**, *6*, 1348−1356.
(70) Arrows illustrating dipole moments point from regions of relative negative to positive charge within the molecule.
(71) Baše, T.; Bastl, Z.; Šlouf, M.; Klementová, M.; Šubrt, J.; Vetushka, A.; Ledinský, M.; Fejfar, A.; Macháček, J.; Carr, M. J.; Londesborough, M. G. S. *J. Phys. Chem. C* **2008**, *112*, 14446−14455.
(72) Lübben, J. F.; Baše, T.; Rupper, P.; Künniger, T.; Macháček, J.; Guimond, S. *J. Colloid Interface Sci.* **2011**, *354*, 168−174.
(73) Kunkel, D. A.; Hooper, J.; Simpson, S.; Miller, D. P.; Routaboul, L.; Braunstein, P.; Doudin, B.; Beniwal, S.; Dowben, P.; Skomski, R.; Zurek, E.; Enders, A. *J. Chem. Phys.* **2015**, *142*, 101921.
(74) Mauguin, C. *Bull. Soc. Fr. Miner.* **1911**, *34*, 71−117.
(75) Fréedericksz, V.; Zolina, V. *Trans. Faraday Soc.* **1933**, *29*, 919−930.
(76) de Jeu, W. H. *Physical Properties of Liquid Crystalline Materials*; Gordon and Breach: New York, 1980.
(77) Fonseca, J. G.; Galerne, Y. *Appl. Phys. Lett.* **2001**, *79*, 2910−2912.
(78) Clare, B. H.; Guzmán, O.; de Pablo, J. J.; Abbott, N. L. *Langmuir* **2006**, *22*, 4654−4659.
(79) Sørensen, B. E. *Eur. J. Mineral.* **2013**, *25*, 5−10.
(80) Lowe, A. M.; Ozer, B. H.; Bai, Y.; Bertics, P. J.; Abbott, N. L. *ACS Appl. Mater. Interfaces* **2010**, *2*, 722−731.
(81) Fukuda, J.; Yoneya, M.; Yokoyama, H. *Phys. Rev. E* **2009**, *79*, 011705.
(82) Choi, Y.; Yokoyama, H.; Gwag, J. S. *Opt. Express* **2013**, *21*, 12135.
(83) Faetti, S.; Marianelli, P. *Phys. Rev. E* **2005**, *72*, 051708.
(84) Anchoring energies depend on a variety of factors. When comparing values from such dissimilar surfaces, one should acknowledge the significant influence of textural and chemical differences in determining anchoring strengths.
(85) Skaife, J. J.; Brake, J. M.; Abbott, N. L. *Langmuir* **2001**, *17*, 5448−5457.
(86) Clare, B. H.; Guzmán, O.; de Pablo, J.; Abbott, N. L. *Langmuir* **2006**, *22*, 7776−7782.
(87) Otiti, T.; Niklasson, G. A.; Svedlindh, P.; Granqvist, C. G. *Thin Solid Films* **1997**, *307*, 245−249.
(88) Everitt, D. L.; Miller, W. J. W.; Abbott, N. L.; Zhu, X. D. *Phys. Rev. B: Condens. Matter Mater. Phys.* **2000**, *62*, R4833−R4836.
(89) Jang, J. H.; Jacob, J.; Santos, G.; Lee, T. R.; Baldelli, S. *J. Phys. Chem. C* **2013**, *117*, 15192−15202.
(90) Smith, H. D.; Obenland, C. O.; Papetti, S. *Inorg. Chem.* **1966**, *5*, 1013−1015.
(91) Plešek, J.; Janoušek, Z.; Heřmánek, S. *Collect. Czech. Chem. Commun.* **1980**, *45*, 1775−1779.
(92) Spokoyny, A. M.; Machan, C. W.; Clingerman, D. J.; Rosen, M. S.; Wiester, M. J.; Kennedy, R. D.; Stern, C. L.; Sarjeant, A. A.; Mirkin, C. A. *Nat. Chem.* **2011**, *3*, 590−596.
(93) Schwartz, J. J.; Hohman, J. N.; Morin, E. I.; Weiss, P. S. *ACS Appl. Mater. Interfaces* **2013**, *5*, 10310−10316.
(94) Goerigk, L.; Grimme, S. *Phys. Chem. Chem. Phys.* **2011**, *13*, 6670−6688.
(95) Hickey, A. L.; Rowley, C. N. *J. Phys. Chem. A* **2014**, *118*, 3678−3687.

DOI: 10.1021/jacs.6b02026
J. Am. Chem. Soc. 2016, 138, 5957−5967